

Electronic Supplementary Information

Reverse microemulsion prepared Ni-Pt catalysts for methane cracking to produce CO_x-free hydrogen

Lu Zhou,* Moussab Harb, Linga Reddy Enakonda, Noor Almana, Mohamed Nejib Hedhili, and Jean Marie Basset*

Experimental

Catalyst preparation:

One microemulsion was prepared by mixing an aqueous solution of Ni(NO₃)₂ and/or H₂PtCl₆ with Triton X-100 surfactant and cyclohexane. The molar ratio of water to surfactant (R_w) and concentrations of Ni(NO₃)₂ and/or H₂PtCl₆ were changed to adjust the final catalysts composition and particles size. The other microemulsion consisting of an aqueous solution of N₂H₄, Triton X-100 and cyclohexane was also prepared with the same R_w value. Both the microemulsions were left stirring for 30 min to obtain an optically clear homogeneous dispersion. The two microemulsions were then mixed with a stirrer for another 5 h. Nitrogen atmosphere was maintained throughout the reaction procedure to ensure the complete removal of oxygen. The precipitate of nanoparticles was separated from the solution by centrifugation. The sample was then washed with ethanol for twice and then dried in vacuum at 110 °C overnight. The bimetallic catalysts are named as Ni_xPt_y, here, while the x and y mean the molar percentage in the final catalysts measured by elemental analysis. Pure nickel and platinum catalyst are named as Ni and Pt.

Characterization:

ICP: The elemental composition of the samples dissolved in H₂SO₄/HNO₃ was determined by inductively coupled plasma atomic emission spectroscopy (ICP–AES) on a Thermo–Electron 3580 instrument.

XRD: XRD patterns were collected using a Bruker D8 Advanced A25 diffractometer in Bragg–Brentano geometry fitted with a copper tube operating at 40 kV and 40 mA and a linear position sensitive detector (opening 2.9°). The diffractometer was configured with a 0.36° diverging slit, 2.9° anti scattering slit, 2.5° Soller slits, and a Ni filter. The data sets were acquired in continuous scanning mode (0.008°/s) over the 2θ range 15–120°, using a step interval of 0.04° and a counting time of 5 s per step.

TEM: TEM samples were prepared by the conventional method of dispersing a small amount of activated/spent catalyst in ethanol and stirring in an ultrasonic bath for 10 min, allowing the homogenized liquid to settle for 5 min and, taking a drop from the top of the vessel to a conventional TEM holder. The nature of the carbon deposit, size and properties were observed using high-resolution transmission electron microscopy (HRTEM) micrographs and also HAADF-STEM obtained from a Titan 60-300 TEM (FEI Co, Netherlands) equipped with an electron emission gun operating at 300 kV. Fast-Fouriertransform (FFT) analysis was applied to various regions of the high-resolution TEM micrographs to investigate the crystal structure of various particles. Dark-field scanning transmission electron microscopy (DF-STEM) was performed on a Titan G 60–300 ST electron microscope at an accelerating voltage of 300 kV to allow dark field imaging using a Gatan STEM detector (model 806). The elemental compositions of the samples were characterized based on the acquisition of spectra from electron energy loss spectroscopy (EELS). A small camera length of 38 mm was selected for imaging and elemental mapping in order to enhance the quality of EELS spectra.

XPS: X-ray photoelectron spectroscopy (XPS) studies were carried out in a Kratos Axis Ultra DLD spectrometer equipped with a monochromatic Al Kα X-ray source (hν = 1486.6 eV) operating at 150 W, a multi-channel plate and delay line detector under a vacuum of ~10⁻⁹ mbar. All spectra were recorded using an aperture slot of 300 μm x 700 μm. Survey spectra were collected using a pass energy of 160 eV and a step size of 1 eV. A pass energy of 20 eV and a step size of 0.1 eV were used for the high-resolution spectra. Samples were mounted in floating mode in order to avoid differential charging. Charge neutralization was required for all samples. Binding energies were referenced to the sp² hybridized (C=C) carbon for the C 1s peak set at 284.4 eV from carbon. The data were analyzed with commercially available software, CASAXPS.

Raman: The Raman spectra of the deposited carbon samples were taken in a Witec Raman spectrometer (Alpha 300R) equipped with a diode Nd:YAG laser and an excitation wavelength of 532 nm from 10 to 4000 cm⁻¹.

TGA: The weight loss due to carbon deposits oxidation was measured by using a thermogravimetric analyzer of METTLER TOLEDO, model TGA/DSC1. The accuracy and precision of temperature and weight measurements of this instrument is ±1.0 and 0.4%, respectively. A 10 mg of sample was kept in the aluminum crucible of the TG analyzer and heated at a rate of 10 °C/min up to 1000 °C in 20 ml/min air flow.

Catalyst activity test:

Activity measurements of the methane cracking process were conducted in a Microactivity Effi reactor from Process Integral Development Eng & Tech S.L. equipped with a long quartz tube reactor (internal diameter: 4 mm; length: 305 mm). First, catalyst (size: 250–300 μm) was loaded into the reactor, and the reaction temperature was controlled by a thermocouple placed in the center of the catalyst layer. Conversions of CH₄ was typically adjusted to be significantly lower than those defined by thermodynamic equilibrium by adjusting the total flow rate. Rate limitation by external and/or internal mass transfer under different conditions proved to be negligible under suitable experimental criteria. The outlet gases were analyzed by online gas chromatography (GC; Varian 450) and micro GC (Soprane MicroGC 3000). The catalyst activity was determined by evaluating the turnover frequency (TOF) of CH₄. The TOF was calculated by

normalizing the reaction rates to the number of exposed surface Ni atoms. The apparent activation energy (E_a) was calculated from the Arrhenius plots of the TOF.

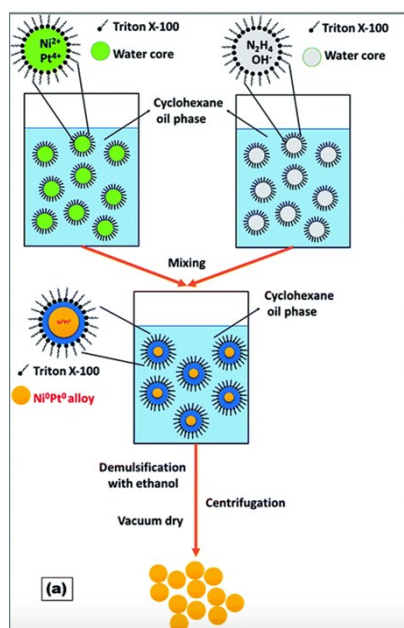


Figure S1. scheme of W/O microemulsion method to prepared Ni-Pt catalysts.

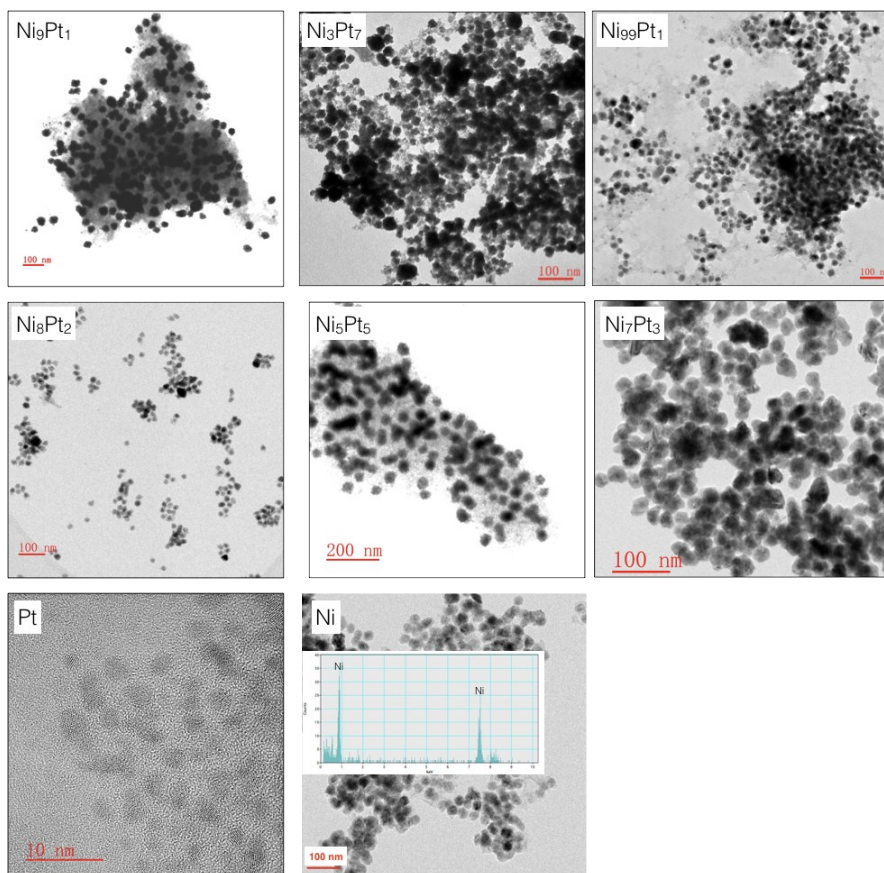


Figure S2. Reverse microemulsion prepared Ni_xPt_y with 30 nm particle size.

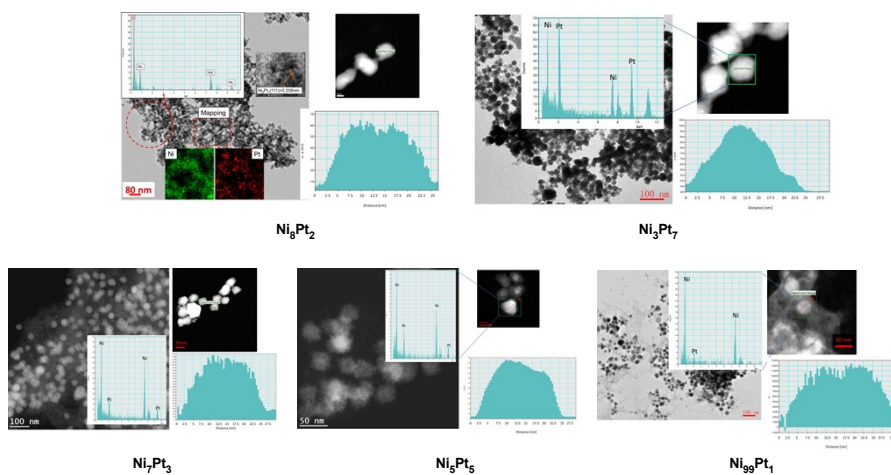


Figure S3. STEM-EDX analysis over Ni_xPt_y samples

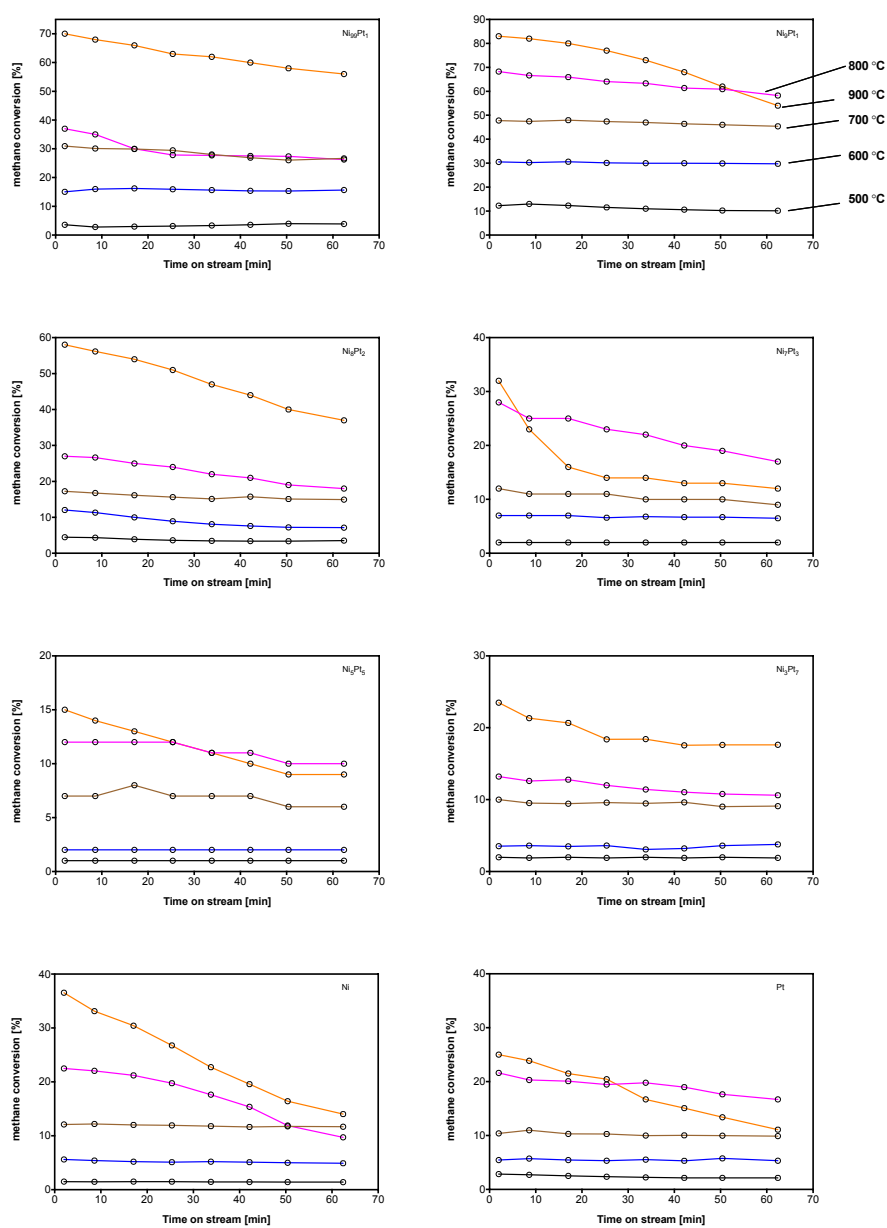


Figure S4. stability testing over Ni_xPt_y samples with crystal size of 30nm (Pt of 3nm)4
 reaction condition: pure CH_4 , space velocity = $0.25 L/g_{cat} \cdot min$.

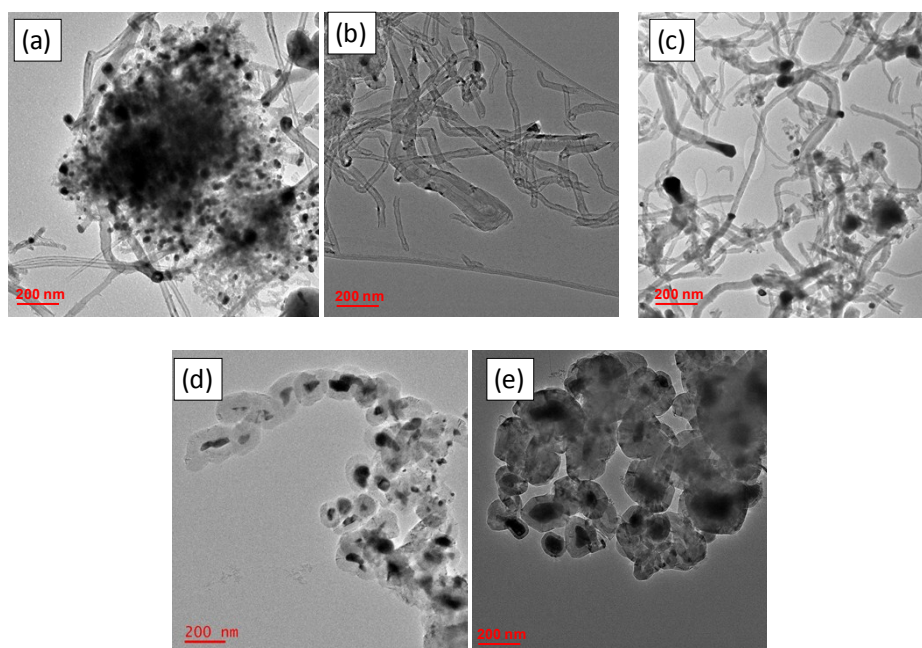


Figure S5. TEM over spent Ni_9Pt_1 after methane cracking at different temperature in Figure S4. (a) 500°C; (b) 600°C; (c) 700°C; (d) 800°C; (e) 900°C. Reaction condition: pure CH_4 , space velocity = 0.25 $\text{L/g}_{\text{cat}} \cdot \text{min}$.

DFT study:

Starting from the commonly observed FCC-derived icosahedral shape of Ni_{55} nanocluster containing 42 atoms on the surface and 13 atoms in the core, we modeled several atomic configurations of bimetallic Ni-Pt nanoclusters by mainly focusing on the two particular Ni/Ni+Pt ratios of 0.5 and 0.9 obtained experimentally in order to help explaining the difference in the measured apparent activation energy. The Ni/Ni+Pt ratios of 0.9 and 0.5 were simulated by respectively substituting 7 and 27 Ni atoms by 7 and 27 Pt atoms at different possible atomic positions into the Ni_{55} nanocluster. We systematically computed for each structural configuration the relative formation energy in order to estimate the most stable structure at room temperature and the structural evolution as a function of temperature treatment. Spin-polarized density functional theory (DFT) together with the plane wave (PW) approach as implemented in the Vienna Ab-initio Simulation Package (VASP) [1-4] were performed for total energy calculations of the various generated bimetallic Ni-Pt nanoalloy structures. The Perdew-Burke-Ernzerhof (PBE) exchange-correlation functional [5] and the Projector-Augmented Plane Wave (PAW) approach [6] were employed to describe the electron-electron and electron-ion interactions, respectively. The convergence criterion for the electronic self-consistent-field (SCF) cycles was fixed at 0.01 meV. The atomic coordinates were fully relaxed until the three components of the Hellmann-Feynman forces on each atom reached values below 0.01 eV \AA^{-1} in order to obtain reliable computed electronic energies of the selected bimetallic Ni-Pt nanoclusters. We show in Figure S6 relevant atomic structures of $\text{Ni}_{48}\text{Pt}_7$ nanocluster with a Ni/Ni+Pt ratio of 0.9 obtained by DFT from a direct substitution of 7 neutral Ni by 7 neutral Pt atoms at different possible positions into the icosahedral Ni_{55} nanocluster. The relative energy together with the corresponding temperature were determined for each structural configuration (given in brackets) in order to evaluate the most stable configuration at room temperature and the structural evolution during heating process. The lowest-energy structural configuration was obtained when all Pt atoms are well dispersed on the surface without the formation of any Pt-Pt bond (see Fig. S6a), highlighting this atomic structure as being energetically the most stable one at room temperature. The structure showing a full Pt segregation on the surface with a maximal number of Pt-Pt bonds was found 32 meV/atom less stable than the previous one (Fig. S6b), indicating the possible appearance of this disposition around 370 K. However, the configurations displaying random alloy-like structures with the majority of Pt are incorporated into the core of the nanocluster and the minority remaining on the surface, as displayed in Fig. S6c and S6d, with computed surface Pt-Ni bonds of 2.56 \AA , were obtained at 71 and 92 meV/atom higher in energy than the lowest-energy one. As a consequence, these atomic dispositions are expected to become significant in the 820-1067 K range, which is very close the one used in the experiment.

The DFT-based key atomic structures of $\text{Ni}_{28}\text{Pt}_{27}$ nanocluster with a Ni/Ni+Pt ratio of 0.5 obtained from a direct substitution of 27 neutral Ni by 27 neutral Pt atoms at different possible Ni sites into the icosahedral Ni_{55} nanocluster, are displayed in Figure S7. The lowest-energy atomic disposition was acquired when all Pt atoms are fully dispersed on the surface with a minimal formation of Pt-Pt bonds (Fig. S7a), indicating this structural configuration as the most stable one at room temperature. However, the structure revealing a complete segregation of Pt on the surface with a maximal number of Pt-Pt bonds was found 37 meV/atom higher in energy

than the previous case (Fig. S7b). This result reveals the possible presence of this configuration around 430 K. Interestingly, the configuration showing a considerable amount of Pt fully segregated on the surface and the other randomly distributed outside and inside the nanocluster (see Fig. S7c) with computed surface Pt-Pt bonds of 2.76 Å and surface Pt-Ni bonds of 2.56 Å, was found 84 meV/atom less stable than the lowest-energy one. As a typical estimate, this atomic disposition will become significant at around 975 K, temperature very close the one adopted in the experiment. Finally, the structure showing random alloy-like disposition, as displayed in Fig. S7d, was found 117 meV/atom higher in energy than the first case, which indicates the possible appearance of this configuration beyond 1300 K.

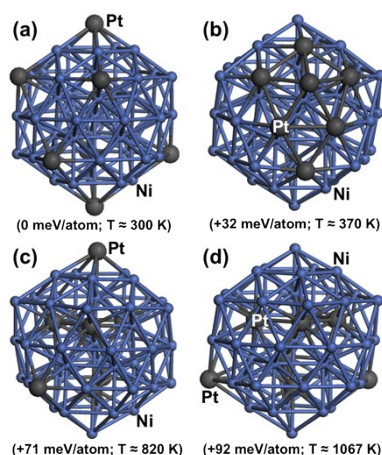


Fig. S6 DFT-relaxed structural configurations of $\text{Ni}_{48}\text{Pt}_7$ nanocluster. For each configuration, the computed relative energy (in meV/atom) and the corresponding estimated temperature are given in brackets. Color legend: Ni in light blue and Pt in dark gray.

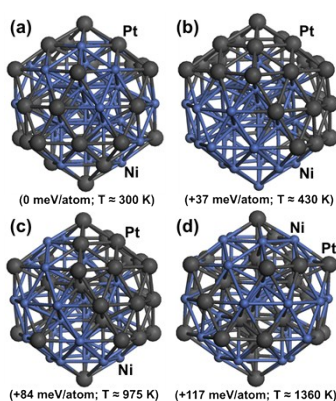


Fig. S7 DFT-optimized structural isomers of $\text{Ni}_{28}\text{Pt}_{27}$ nanocluster. For each configuration, the computed relative energy (in meV/atom) and the corresponding estimated temperature are given in brackets. Color legend: Ni in light blue and Pt in dark gray.

References

- (1) G. Kresse, J. Hafner, *Physical Review B* **1994**, *49*, 14251-14269.
- (2) G. Kresse, J. Furthmüller, *Physical Review B* **1996**, *54*, 11169-11186.
- (3) G. Kresse, J. Furthmüller, *Computational Materials Science* **1996**, *6*, 15-50.
- (4) G. Kresse, D. Joubert, *Physical Review B* **1999**, *59*, 1758-1775.
- (5) J. P. Perdew, K. Burke, M. Ernzerhof, *Physical Review Letters* **1996**, *77*, 3865-3868.
- (6) P. E. Blöchl, *Physical Review B* **1994**, *50*, 17953-17979.